ELSEVIER

Journal of Power Sources 93 (2001) 130–140

JOURNAL OF POWER SOURCES

www.elsevier.com/locate/jpowsour

A complete polarization model of a solid oxide fuel cell and its sensitivity to the change of cell component thickness

S.H. Chan*, K.A. Khor, Z.T. Xia

Fuel Cell Research Group, School of Mechanical and Production Engineering, Nanyang Technological University, Singapore 639798, Singapore

Received 30 May 2000; accepted 8 August 2000

Abstract

This paper presents a complete polarization model of a solid oxide fuel cell (SOFC) that eliminates the ambiguity of the suitability of such model when used under different design and operating conditions. The Butler–Volmer equation is used in the model to describe the activation overpotential instead of using simplified expressions such as the Tafel equation and the linear current–potential equation. In the concentration overpotential, both ordinary and Knudsen diffusions are considered to cater for different porous electrode designs. Sensitivity tests are then conducted to show the effect of the thickness of the respective fuel cell components on the drop in cell voltage. Results show that the performance of an anode-supported fuel cell is superior to that using cathode as the support under elevated operating pressure in the cathode compartment. The former can achieve an improved operating range of current density under normal atmospheric conditions.

Keywords: Solid oxide fuel cell; Anode-supported fuel cell; Cathode-supported fuel cell; Electrolyte-supported fuel cell; Sensitivity test

1. Introduction

Conventional power stations are, in general, based on vapour power (Rankine) cycle or gas turbine (Brayton) cycle, principles for power generation. Thus, the maximum thermal efficiency of such plants is restricted by the Carnot cycle principle. That is to say, the actual thermal efficiency of a plant can be improved either by increasing the steam/gas temperature at the inlet of the steam/gas turbine, or by reducing the discharge temperature at the steam/gas turbine exit. A high inlet temperature is normally restricted by metallurgical considerations, while the low discharge temperature at most can only reach the environmental temperature (or the so-called 'dead state' in the energy analysis). In fact, increasing the inlet temperature of the steam/gas turbine would cause a proportional increase in temperature at the steam/gas turbine exit and heat transfer losses, which yields only a marginal improvement thermal efficiency unless proper recovery of waste heat is adopted.

In recent years, the advantages of gas-turbine integrated fuel-cell power plants with multi-fuel capability that can meet commercial performance goals have been defined [1]. Predicted results have claimed that a thermal efficiency as high as 74% lower heating value (LHV) can be achieved with an integrated gas turbine-heat recovery steam generator (HRSG) and solid oxide fuel cell (SOFC) plant. By contrast, advanced gas turbine-HRSG plant can reach about 62% LHV [2]. All models of fuel cell in the simulation code for predicting the plant efficiency rely extensive experimental data to characterize the polarization curve of the fuel cell sub-system, given that all cells have the same characteristics. It is well-known that the polarization curve is a function of both the operating conditions and the component design of the fuel cell. The operating conditions include the working temperature, partial pressures of the fuel and oxidant and their utilization rate, and the water concentration in the anode compartment. The design specifications include the porosity, tortuosity and thickness of the anode and cathode (responsible for concentration overpotential), the thickness of the electrolyte (responsible for ohmic overpotential), and the electrode/electrolyte interface (responsible for activation overpotential). A complete polarization model, if available, will be extremely useful to characterize the operation of the fuel cell sub-system provided that the design specifications, as mentioned above, are given. In addition, a generalized model would replicate the fuel cell performance reliably under off-design operating conditions such as when the current densities are away from those at the operating power.

* Corresponding author. Tel.: +65-7904-862; fax: +65-7911-859.
E-mail address: mshchan@ntu.edu.sg (S.H. Chan).

0378-7753/01/$ – see front matter
PII: S0378-7753(00)00556-5

Nomenclature

C	concentration (mol m^{-3})
D	diffusion coefficient (m^2 s^{-1})
e	energy of molecular interaction (ergs)
E	voltage (V)
F	Faraday constant (=96485 C mol^{-1})
$\bar{g}$	molar Gibbs free energy (J mol^{-1})
G	Gibbs free energy (J)
$\bar{h}$	molar enthalpy (J mol^{-1})
i	current density (A m^{-2})
i_0	exchange current density (A m^{-2})
i_{oa}	anode exchange current density (A m^{-2})
i_{oc}	cathode exchange current density (A m^{-2})
J	flux (mol s^{-1})
K	equilibrium constant
l_a	anode thickness (m)
l_c	cathode thickness (m)
l_e	electrolyte thickness (m)
M	molecular mass
n	number of moles
n_e	electrons transferred per reaction
p	pressure (Pa)
Q	heat (J)
$\dot{Q}$	heat transfer rate (J s^{-1})
$\bar{r}$	average pore radius (m)
$\bar{R}$	universal gas constant (=8.314 J mol^{-1} K^{-1})
R	area-specific resistance (Ω m^{-2})
R_e	electrolyte area-specific ohmic resistance (Ω m^{-2})
R_{Conc}	area-specific concentration resistance (Ω m^{-2})
$\bar{s}$	molar entropy (J mol^{-1} K^{-1})
S_A	surface area of the porous solid (m^2 kg^{-1})
S_{l_a}	sensitivity of cell voltage due to the change of anode thickness
S_{l_c}	sensitivity of cell voltage due to the change of cathode thickness
S_{l_e}	sensitivity of cell voltage due to the change of electrolyte thickness
$\dot{W}$	rate of work (J s^{-1})
W_{el}	reversible electrical work (J)
T	temperature (K)
v	velocity of the gas molecule (m s^{-1})
X	mole fraction
z	number of electrons participating in the reaction

Greek Letters

β	transfer coefficient
ε	porosity
η	polarization (V)
η_{Act}	activation polarization (V)
η_{Conc}	concentration polarization (V)
η_{Ohm}	ohmic polarization (V)
ρ	resistivity (Ω m)
ρ_B	bulk density of the solid particle (kg m^{-3})
σ	collision diameter (Å)
σ	entropy production (J mol^{-1} K^{-1})
$\dot{\sigma}$	rate of entropy production (J mol^{-1} K^{-1} s^{-1})
σ_e	electrolyte conductivity (S m^{-1})
Ω_D	collision integral based on the Lennard–Jones potential
ξ	tortuosity

Subscripts

a	anode
A	A specie
B	B specie
c	cathode
cv	control volume
H_2	hydrogen
H_2O	water vapour
i	mixture component
k	Knudsen diffusion
N_2	nitrogen
O_2	oxygen
P	products
R	reactants
(eff)	effective

Superscripts

I	inlet condition

Very often, the Tafel equation or the linear current–voltage relation is used to replace the Butler–Volmer equation in the calculation of activation overpotential. Or, the Knudsen diffusion is neglected in the gas diffusion through the porous electrodes. To avoid the ambiguity of the suitability of such models used in the calculation of cell polarization, the Butler–Volmer equation is retained and both the ordinary and Knudsen diffusions are considered in the proposed polarization model. The development of this model forms the basis of the objective of work presented here. In addition, an analysis is conducted to show the sensitivity of the cell voltage drop on changes in the thickness of respective cell components under fixed exchange current densities.

2. Thermodynamic principles

A fuel cell is just like any other energy conversion device/system in that its performance can be assessed by the principles of thermodynamics [3,4]. Treating the fuel cell as a control volume and applying the steady flow energy equation with the assumption of negligible change of kinetic energy and potential energy gives

$$\dot{Q}_{cv} - \dot{W}_{cv} + \sum_i (\dot{n}_i \bar{h}_i)_R - \sum_i (\dot{n}_i \bar{h}_i)_P = 0 \quad (1)$$

The entropy balance for the control volume can be written as

$$\frac{\dot{Q}_{cv}}{T} - \sum_i (\dot{n}_i \bar{s}_i)_R - \sum_i (\dot{n}_i \bar{s}_i)_P + \dot{\sigma}_{cv} = 0 \quad (2)$$

Combining Eqs. (1) and (2) and assuming that the electrochemical reaction is based on unit molar flow rate of the fuel (for example H_2), yields

$$W_{cv} = -\left[\sum_i (n_i \bar{g}_i)_P - \sum_i (n_i \bar{g}_i)_R\right] - T\sigma_{cv} = 0 \quad (3)$$

where $\bar{g}_i(T, p_i) = \bar{h}_i(T) - T\bar{s}_i(T, p_i)$ or $\bar{g}_i(T, p_i) = \bar{g}_i^0(T) + \bar{R}T \ln(p_i^I/p_0)$Since there is no mechanical work involved in the fuel cell, W_{cv} is naturally the electrical work done by the fuel cell. That is

$$W_{el} = zFE = -\left[\sum_i (n_i \bar{g}_i)_P - \sum_i (n_i \bar{g}_i)_R\right] - T\sigma_{cv} \quad (4)$$

$$zFE = -\Delta G^0 - \left[\sum_i \left(n_i \bar{R}T \ln \frac{p_i^I}{p_0}\right)_P - \sum_i \left(n_i \bar{R}T \ln \frac{p_i^I}{p_0}\right)_R\right] - T\sigma_{cv} \quad (5)$$

where $-\Delta G^0 = \bar{R}T \ln K(T)$.

For a hydrogen fuel cell with known pressures of reactants and product

$$E = \frac{\bar{R}T}{2F} \ln K - \frac{\bar{R}T}{4F} \ln \left[\frac{(p_{H_2O}^I)^2 p_0}{(p_{H_2}^I)^2 p_{O_2}^I}\right] - \frac{\sigma_{cv} T}{2F} \quad (6)$$

where $\sigma_{cv}T/2F = \eta_{Act} + \eta_{Ohm} + \eta_{Conc}$.

The first term on the right-hand side of Eq. (6) shows the effect of the temperature on the cell voltage while the second term shows the effect of the pressures of the reactants and product on cell voltage. The irreversibility in the voltage drop is accounted by the third term of the equation and is expressed by the activation, ohmic and concentration overpotentials.

2.1. Activation polarization

Chemical reactions, including electrochemical reactions, involve energy barriers which must be overcome by the reacting species. This energy barrier is called the 'activation energy' and results in activation or charge-transfer polarization, which is due to the transfer of charges between the electronic and the ionic conductors. The activation polarization may be regarded as the extra potential necessary to overcome the energy barrier of the rate-determining step of the reaction to a value such that the electrode reaction proceeds at a desired rate.

Activation polarization is normally expressed by the well-known Butler–Volmer equation [5]

$$i = i_0 \left\{\exp\left(\beta \frac{n_e F \eta_{Act}}{\bar{R}T}\right) - \exp\left[-(1-\beta)\frac{n_e F \eta_{Act}}{\bar{R}T}\right]\right\} \quad (7)$$

where β is the transfer coefficient and i_0 the exchange current density. The transfer coefficient is considered to be the fraction of the change in polarization that leads to a change in the reaction rate constant, and its value is usually 0.5 for the fuel cell application. The exchange current density is the forward and reverse electrode reaction rate at the equilibrium potential. A high exchange current density means that a high electrochemical reaction rate and good fuel cell performance can be expected.

When $\beta = 0.5$, Eq. (7) can be expressed as follows:

$$i = 2i_0 \sinh\left(\frac{n_e F \eta_{Act}}{2\bar{R}T}\right) \quad (8)$$

Then,

$$\eta_{Act} = \frac{2\bar{R}T}{n_e F} \sinh^{-1}\left(\frac{i}{2i_0}\right) \quad (9)$$

Two special cases of Eq. (7) are available: (1) high activation polarization; (2) low activation polarization.

Under high activation polarization, the first exponential term in Eq. (7) will be much greater than the second term, and the latter can be excluded from the equation. Rearranging the simplified equation yields

$$\eta_{Act} = -\left(\frac{\bar{R}T}{\beta n_e F}\right) \ln i_0 + \left(\frac{\bar{R}T}{\beta n_e F}\right) \ln i \quad (10)$$

which is the well-known Tafel equation.

Under low activation polarization, the term $\beta\eta_{Act}F/\bar{R}T$ in Eq. (7) will be much less than unity and the exponential terms can be expanded as a Taylor series. Neglecting the terms with order higher than unity yields

$$\eta_{Act} = \frac{\bar{R}T}{n_e F i_0} i \quad (11)$$

which is the well-known linear current–potential relation.

It is common to question the range of activation polarization to which the Tafel equation and linear current–potential relation apply. Thus, a plot to display the errors of the simplified activation models relative to the Butler–Volmer equation will be useful. The errors of the Tafel equation and the linear current–potential relation relative to the Butler–Volmer equation at 1073 K are given in Fig. 1. It clearly shows the applicable ranges of these simplified models. For example, if 5% of error is allowed, which corresponds to $\eta_{Act} > 0.28$ V, Tafel equation can be used; however, if $\eta_{Act} < 0.1$ V, the linear relation can be used. For a SOFC, the former is normally applied to the cathode activation, while the latter is normally applied to the anode activation.

2.2. Ohmic polarization

Ohmic losses occur because of resistance to the flow of ions in the electrolyte and resistance to flow of electrons through the electrode materials. The dominant ohmic losses, through the electrolyte, can be reduced by decreasing the

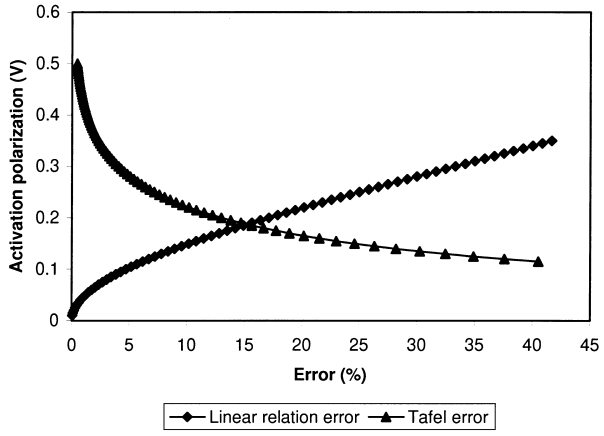

Fig. 1. Error of Tafel and linear relation results relative to Butler–Volmer equation at 1073 K.

distance of electrode separation and enhancing the ionic conductivity of the electrolyte. Because the ionic flow in the electrolyte obeys Ohm's law, the ohmic losses can be expressed by the equation

$$\eta_{\text{Ohm}} = iR_{\text{e}} \tag{12}$$

where R_{e} is the ionic resistance.

2.3. Concentration polarization

The rate of mass transport to the reaction sites in a porous electrode of a SOFC can be described by the diffusion of gases in the pores. The gases have to diffuse through the gas-filled pores of the electrode in order to reach the reaction sites. Whenever this happens, it is possible for the concentration polarization to be significant, since when the current is being drawn the gas partial pressure at the reaction sites will be less than that in the bulk of the gas stream. Hence, decrease of gas concentration in the gas-filled pores of the electrode may give rise to severe polarization and lead to limiting current. Normal concentration polarization does not give rise to excessive voltage losses until the current densities approach the limiting current.

Diffusion through the porous material is typically described by either ordinary or Knudsen diffusion and has been found to play an important role in catalytic reaction. Ordinary diffusion occurs when the pore diameter of the material is large in comparison to the mean free path of the gas molecules. Molecular transport through pores which are small in comparison to the mean free path of the gas is regarded as a Knudsen type of diffusion. For Knudsen diffusion, molecules collide more frequently with the pore walls than with other molecules. Upon collision, the atoms are instantly adsorbed on to the surface and are then desorbed in a diffusive manner. As a result of frequent collisions with the wall of the pore, the transport of the molecule is impeded. The Knudsen diffusion coefficient can be predicted using kinetic theory by relating the diameter of the pore and the mean free path of the gas [6]

$$D_{\text{k}} = \frac{v\bar{r}}{6} \tag{13}$$

For straight and round pores, the diffusion coefficient of the A component becomes

$$D_{\text{Ak}} = 97.0\bar{r}\sqrt{\frac{T}{M_{\text{A}}}} \tag{14}$$

The mean pore radius can be evaluated from the bulk density, the surface area of the porous solid, and the porosity by the expression

$$\bar{r} = \frac{2\varepsilon}{S_{\text{A}}\rho_{\text{B}}} \tag{15}$$

To account for the tortuous path of the molecule rather than along the radial direction and the porosity of the solid electrode for the fact that diffusion occurs only in the pore space, an effective Knudsen diffusion coefficient may be used, i.e.

$$D_{\text{Ak(eff)}} = D_{\text{Ak}}\left(\frac{\varepsilon}{\xi}\right) \tag{16}$$

Using the Chapman–Enskog theory of prediction, the binary ordinary diffusion coefficient in the gas phase can be calculated [7] as follows:

$$D_{\text{AB}} = 0.0018583\left(\frac{1}{M_{\text{A}}} + \frac{1}{M_{\text{B}}}\right)^{1/2}\frac{T^{3/2}}{p\sigma_{\text{AB}}^2\Omega_{\text{DAB}}} \tag{17}$$

where p is the total pressure (in atm), $\sigma_{\text{AB}} = (\sigma_{\text{A}} + \sigma_{\text{B}})/2$ is the collision diameter (in Å) and Ω_{DAB} is the collision integral based on the Lennard–Jones potential which can be obtained from e_{AB}. e_{AB} is the energy of molecular interaction in ergs ($e_{\text{AB}}/k = \sqrt{(e_{\text{A}}/k)(e_{\text{B}}/k)}$, K).

Similar to the Knudsen diffusion, the effective diffusion coefficient for ordinary diffusion can be described by the following equation:

$$D_{\text{AB(eff)}} = D_{\text{AB}}\left(\frac{\varepsilon}{\xi}\right) \tag{18}$$

Both ordinary diffusion and Knudsen diffusion may occur simultaneously. For self-diffusion or equimolar counter transfer, the effective diffusion coefficient can be written as

$$\frac{1}{D_{\text{A(eff)}}} = \frac{1}{D_{\text{AB(eff)}}} + \frac{1}{D_{\text{Ak(eff)}}} \tag{19a}$$

and

$$\frac{1}{D_{\text{A(eff)}}} = \frac{\xi}{\varepsilon}\left(\frac{1}{D_{\text{AB}}} + \frac{1}{D_{\text{Ak}}}\right) \tag{19b}$$

In this context, the combined effect of both types of diffusion on concentration polarization is considered. If it is assumed that the pores of different sizes are highly interlinked and randomly arranged, then it can be assumed that the path of any molecule transfers through the solid electrode should involve essentially the same flow resistance as the path of any other molecules.

2.3.1. Anode — equimolar counter-current diffusion of reactant and product

On the anode side, the chemical reaction occurs at the end of the diffusion path. The flux ratios at steady-state are determined by the stoichiometry of the reaction. Therefore,

$$J = J_{H_2} + J_{H_2O} = 0 \tag{20}$$

Since the mass of hydrogen diffusion in one direction does not necessarily equal the mass diffusion in the other direction, a definite net mass flow in one direction is present. The equations of diffusion are

$$J_{H_2} = -D_{H_2(eff)}\nabla C_{H_2} + C_{H_2}v \tag{21a}$$

$$J_{H_2O} = -D_{H_2O(eff)}\nabla C_{H_2O} + C_{H_2O}v \tag{21b}$$

where

$$\frac{1}{D_{H_2(eff)}} = \frac{1}{D_{H_2,k(eff)}} + \frac{1}{D_{H_2-H_2O(eff)}}$$

$$\frac{1}{D_{H_2O(eff)}} = \frac{1}{D_{H_2O,k(eff)}} + \frac{1}{D_{H_2-H_2O(eff)}}$$

For steady state conditions, $\nabla C_{H_2} = -\nabla C_{H_2O}$, Eqs. (21a) and (21b) become

$$J_{H_2} = -D_{H_2(eff)}\nabla C_{H_2} + C_{H_2}v \tag{22a}$$

$$J_{H_2O} = D_{H_2O(eff)}\nabla C_{H_2} + C_{H_2O}v \tag{22b}$$

For equimolar counter-current mass transfer, $J_{H_2} = -J_{H_2O}$

$$-(D_{H_2(eff)} - D_{H_2O(eff)})\nabla C_{H_2} + v(C_{H_2} + C_{H_2O}) = 0 \tag{23a}$$

or

$$v = \frac{D_{H_2(eff)} - D_{H_2O(eff)}}{C_a}\nabla C_{H_2} \tag{23b}$$

where $C_a = C_{H_2} + C_{H_2O}$.

Substituting into Eqs. (21a) and (21b), gives

$$J_{H_2} = -\left[\left(\frac{C_{H_2O}}{C_a}\right)D_{H_2(eff)} + \left(\frac{C_{H_2}}{C_a}\right)D_{H_2O(eff)}\right]\nabla C_{H_2} \tag{24a}$$

$$J_{H_2O} = -\left[\left(\frac{C_{H_2O}}{C_a}\right)D_{H_2(eff)} + \left(\frac{C_{H_2}}{C_a}\right)D_{H_2O(eff)}\right]\nabla C_{H_2O} \tag{24b}$$

or

$$J_{H_2} = -D_{a(eff)}\nabla C_{H_2} \tag{25a}$$

$$J_{H_2O} = -D_{a(eff)}\nabla C_{H_2O} \tag{25b}$$

where

$$D_{a(eff)} = \left(\frac{C_{H_2O}}{C_a}\right)D_{H_2(eff)} + \left(\frac{C_{H_2}}{C_a}\right)D_{H_2O(eff)}$$

or

$$D_{a(eff)} = \left(\frac{p_{H_2O}}{p_a}\right)D_{H_2(eff)} + \left(\frac{p_{H_2}}{p_a}\right)D_{H_2O(eff)}$$

Since the difference between $D_{H_2(eff)}$ and $D_{H_2O(eff)}$ is not very large, when the hydrogen partial pressure does not change critically, $D_{a(eff)}$ may be considered as a constant.

For one-dimensional diffusion,

$$J_{H_2} = -D_{a(eff)}\frac{dC_{H_2}}{dl} \tag{26}$$

Because $J_{H_2} = -(i/2F)$ and $dC_{H_2} = (dp_{H_2}/\bar{R}T)$, so,

$$dp_{H_2} = \frac{\bar{R}Ti}{2FD_{a(eff)}}\,dl \tag{27a}$$

Integrating this equation with the boundary condition $p_{H_2} = p^I_{H_2}$ at anode surface yields

$$p_{H_2} - p^I_{H_2} = \frac{\bar{R}Ti}{2FD_{a(eff)}}l_a \tag{27b}$$

Therefore, in terms of the current density, i, partial pressure of hydrogen, p_{H_2}, and water vapour partial pressure, p_{H_2O}, at reaction sites

$$p_{H_2} = p^I_{H_2} - \frac{\bar{R}Tl_a}{2FD_{a(eff)}}i \tag{28a}$$

$$p_{H_2O} = p^I_{H_2O} + \frac{\bar{R}Tl_a}{2FD_{a(eff)}}i \tag{28b}$$

where

$$\frac{1}{D_{H_2(eff)}} = \frac{\xi_a}{\varepsilon_a}\left(\frac{1}{D_{H_2,k}} + \frac{1}{D_{H_2-H_2O}}\right)$$

$$\frac{1}{D_{H_2O(eff)}} = \frac{\xi_a}{\varepsilon_a}\left(\frac{1}{D_{H_2O,k}} + \frac{1}{D_{H_2-H_2O}}\right)$$

2.3.2. Cathode — self-diffusion

On the cathode side, the flux of nitrogen is zero. Thus [5],

$$J_{O_2} = -D_c\nabla C_{O_2} + X_{O_2}\delta_{O_2}J_{O_2} \tag{29}$$

where

$$\delta_{O_2} = \frac{D_{O_2,k(eff)}}{D_{O_2,k(eff)} + D_{O_2-N_2(eff)}}$$

For one-dimensional diffusion,

$$J_{O_2} = -D_{O_2(eff)}\frac{dC_{O_2}}{dl} + X_{O_2}\delta_{O_2}J_{O_2} \tag{30}$$

Because $J_{O_2} = -i/4F$ and $dC_{O_2} = dp_{O_2}/\bar{R}T$, so

$$\frac{dp_{O_2}}{p_c - \delta_{O_2}p_{O_2}} = \frac{\bar{R}Ti}{4FD_{O_2(eff)}p_c}\,dl \tag{31a}$$

Integrating this equation with the boundary condition $p_{O_2} = p^I_{O_2}$ at cathode surface yields

$$\ln\left(\frac{(p_c/\delta_{O_2}) - p_{O_2}}{(p_c/\delta_{O_2}) - p^I_{O_2}}\right) = \frac{\delta_{O_2}\bar{R}Ti}{4FD_{O_2(eff)}p_c}l_c \tag{31b}$$

Therefore, the partial pressure of oxygen at the cathode reaction sites is

$$p_{O_2} = \frac{p_c}{\delta_{O_2}} - \left(\frac{p_c}{\delta_{O_2}} - p^I_{O_2}\right)\exp\left(\frac{\delta_{O_2}\bar{R}Til_c}{4FD_{c(eff)}p_c}\right) \quad (32)$$

where

$$\frac{1}{D_{O_2(eff)}} = \frac{\xi_c}{\varepsilon_c}\left(\frac{1}{D_{O_2,k}} + \frac{1}{D_{O_2-N_2}}\right)$$

and

$$D_{c(eff)} = D_{O_2(eff)}$$

3. Overall cell potential

Polarization is a very important parameter in the analysis of fuel cell performance. For calculating the relationship between voltage and current density, the following general expression can be used:

$$E(i) = E_0 - \eta_{Ohm} - \eta_{Act,a} - \eta_{Act,c} - \eta_{Conc,a} - \eta_{Conc,c} \quad (33a)$$

where

$$E_0 = \frac{\bar{R}T}{2F}\ln K - \frac{\bar{R}T}{4F}\ln\left(\frac{(p^I_{H_2O})^2 p_0}{(p^I_{H_2})^2 p^I_{O_2}}\right) \quad (33b)$$

$$\eta_{Ohm} = iR_e \quad (33c)$$

$$\eta_{Act,a} = \frac{2\bar{R}T}{n_eF}\sinh^{-1}\left(\frac{i}{2i_{oa}}\right) \quad (33d)$$

$$\eta_{Act,c} = \frac{2\bar{R}T}{n_eF}\sinh^{-1}\left(\frac{i}{2i_{oc}}\right) \quad (33e)$$

$$\eta_{Conc,a} = -\frac{\bar{R}T}{2F}\ln\left[\frac{(1-(\bar{R}T/2F)(l_a/D_{a(eff)}p^I_{H_2})i}{(1+(\bar{R}T/2F)(l_a/D_{a(eff)}p^I_{H_2O})i}\right] \quad (33f)$$

$$\eta_{Conc,c} = -\frac{\bar{R}T}{4F}\ln\left[\frac{(p_c/\delta_{O_2}) - ((p_c/\delta_{O_2}) - p^I_{O_2})\exp[(\bar{R}T/4F)(\delta_{O_2}l_c/D_{c(eff)}p_c)i]}{p^I_{O_2}}\right] \quad (33g)$$

Some experimental data extracted from the literature [8–10] is presented in Table 1. Note that these performance-related data are extracted from literature which focuses on the development of intermediate temperature SOFCs that operate at a temperature around 800°C [8–10]. Based on these data, the respective polarization curves can be generated.

Table 1
Calculation based parameters for solid oxide fuel cell

Parameter	Value
Fuel cell operating temperature (T) (K)	1073
Fuel cell operating pressure (p) (atm)	1
Hydrogen humidified temperature (T_H) (K)	298
Electrolyte conductivity (σ_e) (S m^{-1})	10
Electron transferred per reacting (n_e)	1
Transfer coefficient (β)	0.5
Anode exchange current density (i_{oa}) (A m^{-2})	5300
Cathode exchange current density (i_{oc}) (A m^{-2})	2000
Cathode thickness (l_c) (m)	50×10^{-6}
Porosity (ε) (%)	30
Tortuosity (ξ)	6
Average pore radius ($\bar{r}$) (m)	0.5×10^{-6}
For electrolyte-supported cell	
Electrolyte thickness (l_e) (m)	500×10^{-6}
Anode thickness (l_a) (m)	50×10^{-6}
For anode-supported cell	
Electrolyte thickness (l_e) (m)	40×10^{-6}
Anode thickness (l_a) (m)	750×10^{-6}

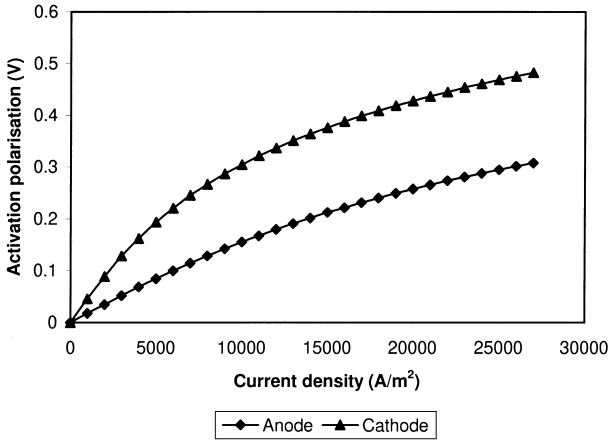

Fig. 2. Calculated activation polarization of solid oxide fuel cell.

3.1. Activation polarization

Calculated anode and cathode activation polarization curves are shown in Fig. 2. The cathode polarization is obviously higher than that of the anode due to its lower exchange current density. The activation polarization increases steeply at low current density and gradually at high current density. The convex-up curvature of polarization is the cause for the concave voltage versus current density trace. It should be noted that the activation loss in the present study was assumed to occur at the electrode/electrolyte interface (or two-dimensional). In an actual fuel cell, the electrochemical reaction occurs at electrochemical active sites (i.e. three-dimensional) where the reactive gas, the electronic conductor and the ionic conductor are present at the same time. In other words, the thickness of the electrode does have an effect of the activation loss, which is

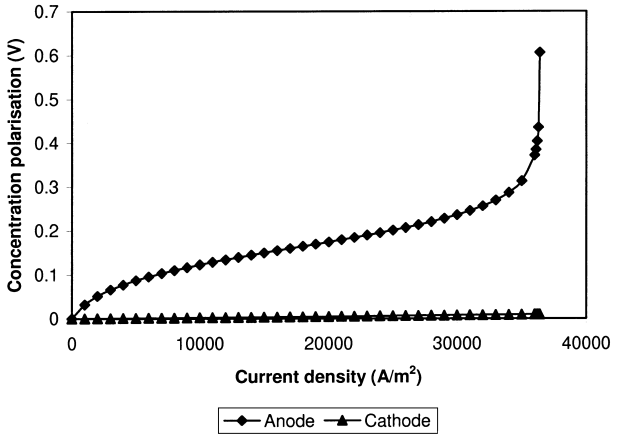

Fig. 3. Calculated concentration polarization of anode-supported solid oxide fuel cell.

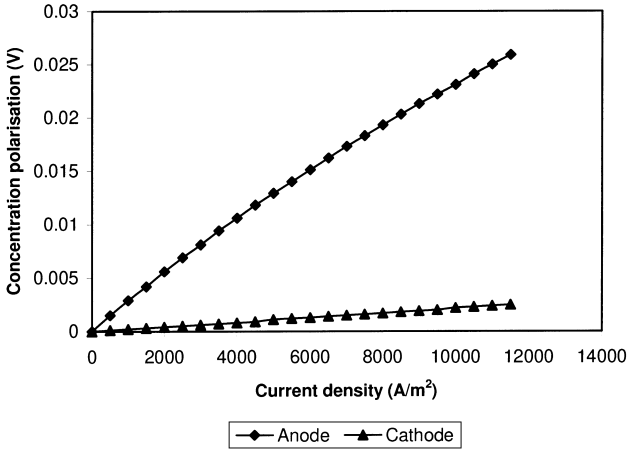

Fig. 4. Calculated concentration polarization of electrolyte-supported solid oxide fuel cell.

ignored in the present study. The present model, however, can be extended to cover the micro level of electrode kinetics based on the work of Costamagna et al. [11].

3.2. Concentration polarization

Anode concentration polarization and cathode concentration polarization are calculated using Eqs. (33f) and (33g), respectively. The calculated concentration polarization of an anode-supported SOFC is shown in Fig. 3. The anode concentration polarization is much higher than that of the cathode because of the thick anode used. It should be noted that the polarization curve is convex at low current density. At high current density, the polarization curve exhibits a concave curvature. Whether or not a concave curvature is observed at high current density (in the cell voltage–current density trace) depends really on the magnitude of the ohmic and activation polarization. For the data in Table 1, the cell voltage drops to zero when the current density reaches 26,600 A m^{-2}. Therefore, this phenomenon (concave curvature) cannot be seen. Actually, the selected parameters of exchange current densities, electrolyte conductivity and thickness are amongst the highest values obtained from the literature. It can be concluded that the anode limiting current density is not reached under normal conditions.

The calculated concentration polarization of an electrolyte-supported SOFC is given in Fig. 4. The curve is slightly convex over the whole range of current density. Because its magnitude is small, it will not influence the shape of the cell voltage versus current density trace.

3.3. Cell voltage and power density

The cell voltage and power densities are calculated for the whole range of fuel cell operations from $i = 0$ to $V = 0$.

The calculated cell voltage, polarization and power density versus current density trace of the electrolyte-supported cell are presented in Fig. 5. The power density reaches a peak value when the current density is 5500 A m^{-2}. At this point, the voltage is 0.519 V and the power density is 2834 W m^{-2}. Normally, the fuel cells are designed to operate slightly left to this point for a good compromise between cell efficiency and low capital cost and the consideration of operational stability. Under this condition, the maximum loss is due to the electrolyte ohmic polarization, and the cathode and anode activation losses are also considerable. The concentration losses are relatively small in this case. When the current density reaches 11,500 A m^{-2}, the cell voltage drops to zero. From this study, one may identify the right polarization to be focused on for improvement. The electrode-supported cells, which have thinner electrolyte,

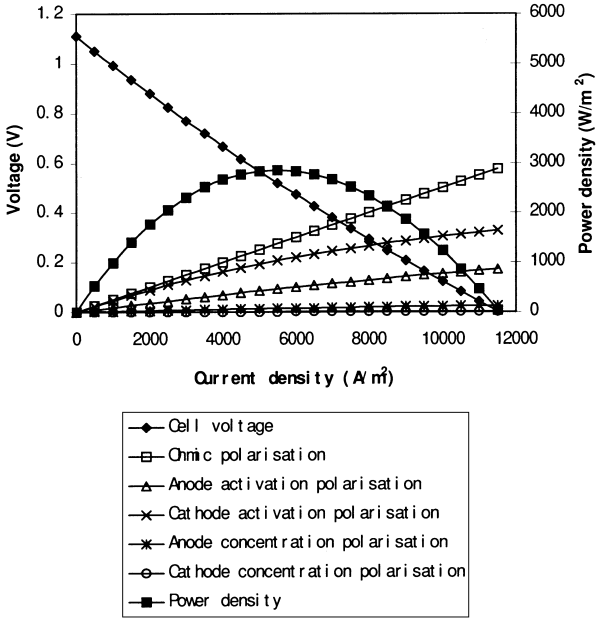

Fig. 5. Calculated cell voltage, polarization and power density vs. current density trace of electrolyte-supported cells.

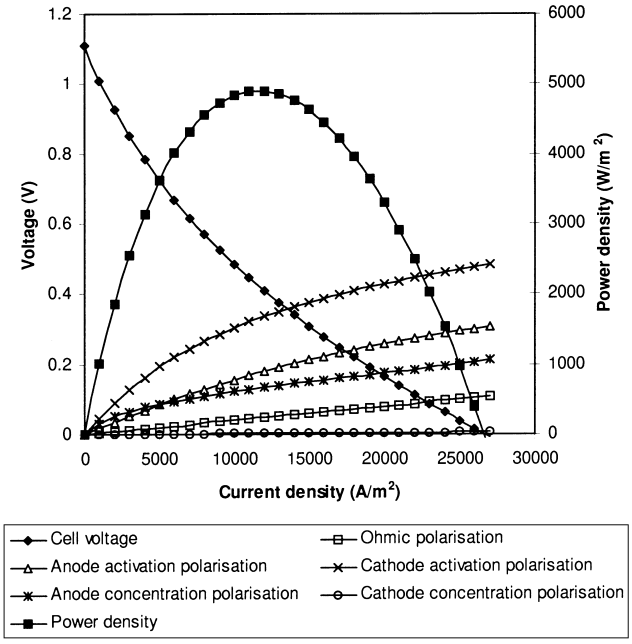

Fig. 6. Calculated cell voltage, polarization and power density vs. current density trace of anode-supported cells.

could have better performance than that of electrolyte-supported cells.

The calculated cell voltage, and power density versus current density trace of an anode-supported cell are given in Fig. 6. As discussed above, it can be concluded that the concave curvature of the cell voltage is due to both activation and concentration polarization. The power density reaches a peak value when the current density is 12,000 A m^{-2}. At this point, the voltage is 0.41 V and the power density is 4900 W m^{-2}. Under such condition, the maximum loss is due to the cathode activation polarization and the anode activation and concentration losses are also significant. The electrolyte ohmic and cathode concentration losses are relatively small. When the current density reaches 26,600 A m^{-2}, the voltage drops to zero. Therefore, the electrode material-related factors such as the catalytic activity and reaction sites, which determine the magnitude of the exchange current density, should be targetted for improvement.

Comparing the structure of anode-supported and electrolyte-supported cells, the only difference is the thickness of the anode and the electrolyte. Therefore, in general, it can be concluded that the performance of anode-supported cells should be better than that of electrolyte-supported cells.

It should be noted, at this point, that the effects of the porosity, tortousity and pore size of the electrodes on the fuel cell performance are not considered because the present model does not examine the effects of these parameters on the effective electrochemical reaction sites. Hence, it is not appropriate to show their effects on the concentration overpotential without considering their impacts on the electrochemical reaction. As mentioned in Section 3.1, once the microelectrode kinetic model is included, the interaction between the activation and concentration overpotentials due to the change of porosity, tortousity and pore size will be meaningful.

4. Sensitivity analysis

The sensitivity study of the proposed model is performed by defining the dimensionless sensitivity of the cell voltage subject to the change of any parameter of interest (P_i)

$$S_{P_i} = \frac{\partial E/E}{\partial P_i/P_i} \tag{34}$$

For a change in anode thickness

$$S_{l_a} = \frac{\partial E/\partial l_a}{E/l_a} \tag{35a}$$

where

$$\frac{\partial E}{\partial l_a} = -\left(\frac{\bar{R}T}{2F}\right)^2 \left(\frac{i}{D_{a(eff)}}\right) \left[\frac{1}{p^I_{H_2O} - (\bar{R}T/2F)(i/D_{a(eff)})l_a} + \frac{1}{p^I_{H_2O} + (\bar{R}T/2F)(i/D_{a(eff)})l_a}\right] \tag{35b}$$

For a change in electrolyte thickness,

$$S_{l_e} = \frac{\partial E/\partial l_e}{E/l_e} \tag{36a}$$

where

$$\frac{\partial E}{\partial l_e} = \frac{i}{\sigma_e l_e^2} \tag{36b}$$

For a change in cathode thickness,

$$S_{l_c} = \frac{\partial E/\partial l_c}{E/l_c} \tag{37a}$$

where

$$\frac{\partial E}{\partial l_c} = -\left(\frac{\bar{R}T}{4F}\right)^2 \frac{(1 - (p^I_{O_2}/p_c)\delta_{O_2}) \exp[(\bar{R}T/4Fp_c)(\delta_{O_2} l_c/D_{c(eff)})i](i/D_{c(eff)})}{(p_c/\delta_{O_2}) - ((p_c/\delta_{O_2}) - p^I_{O_2}) \exp[(\bar{R}T/4Fp_c)(\delta_{O_2} l_c/D_{c(eff)})i]} \tag{37b}$$

The sensitivity of the cell voltage due to the change of respective cell component thickness at different current densities is shown in Figs. 7–11. When all three cell

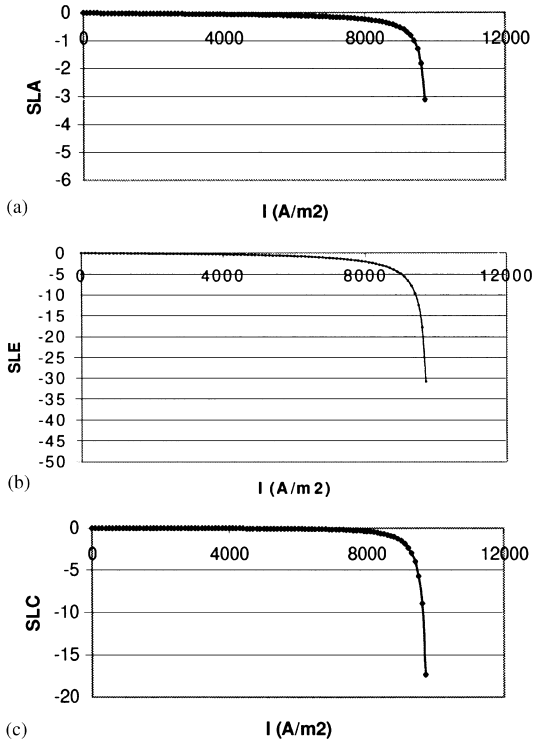

Fig. 7. (a) Sensitivity of cell voltage due to anode thickness (anode/cathode/electrolyte: 500 μm). (b) Sensitivity of cell voltage due to electrolyte thickness (anode/cathode/electrolyte: 500 μm). (c) Sensitivity of cell voltage due to cathode thickness (anode/cathode/electrolyte: 500 μm).

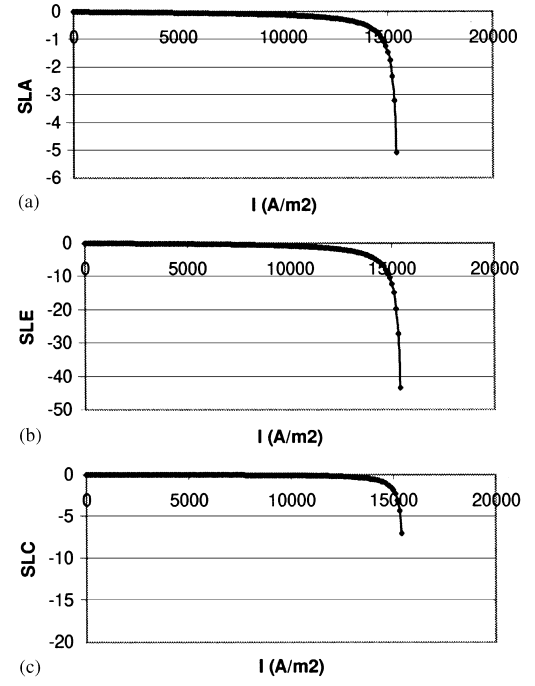

Fig. 8. (a) Sensitivity of cell voltage due to anode thickness (anode/cathode/electrolyte: 250 μm). (b) Sensitivity of cell voltage due to electrolyte thickness (anode/cathode/electrolyte: 250 μm). (c) Sensitivity of cell voltage due to cathode thickness (anode/cathode/electrolyte: 250 μm).

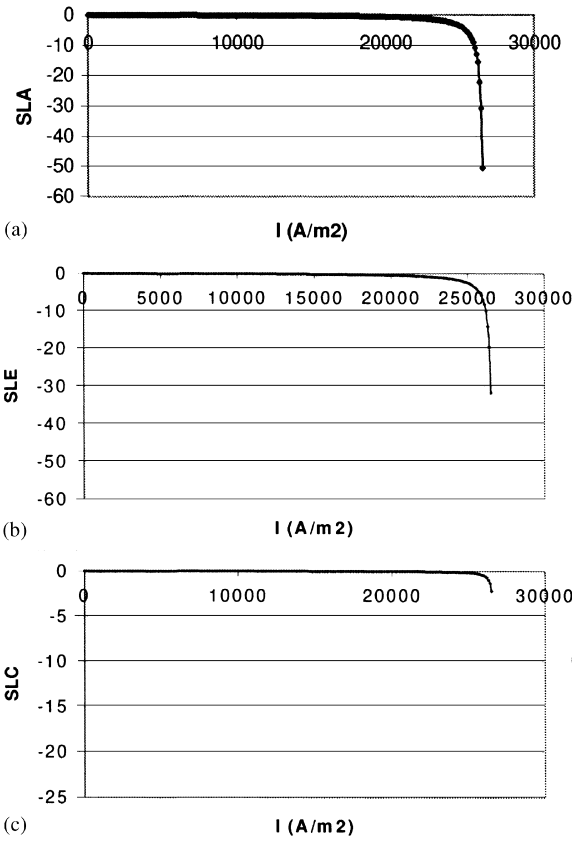

Fig. 9. (a) Sensitivity of cell voltage due to anode thickness (anode: 750 μm; cathode: 50 μm; electrolyte: 40 μm). (b) Sensitivity of cell voltage due to electrolyte thickness (anode: 750 μm; cathode: 50 μm; electrolyte: 40 μm). (c) Sensitivity of cell voltage due to cathode thickness (anode: 750 μm; cathode: 50 μm; electrolyte: 40 μm).

components, namely, anode, cathode and electrolyte, have the same thickness of 500 μm (Fig. 7a–c), S_{l_e} is the largest, then S_{l_c} and finally S_{l_a}. Decreasing all three thicknesses to 250 μm (Fig. 8a–c), in general, results in reduced sensitivities and an improved operating current density range. Intuitively, these sensitivity profiles show that the use of electrolyte as the fuel cell support is not as good as that using either anode or cathode as the support. The sensitivity profiles of anode-supported and cathode-supported cells are compared in Figs. 9 and 10, respectively, The results show that the anode-supported cell is superior to the cathode-supported cell in terms of operating current density range and, hence, higher power density can be achieved. It is obvious that anode concentration overpotential is the cause of limiting current for the former, whereas cathode concentration overpotential is the cause of limiting current for the latter. To compensate for the serious cathode concentration overpotential loss in the cathode-supported cell, the cathode compartment pressure is increased from atmospheric pressure to 4 bar. In general, all three sensitivities are reduced with improved operating current density range, see Fig. 11a–c. Compared with an anode-supported cell operating at atmospheric condition, however, the cathode-supported cell is no way better in terms of performance.

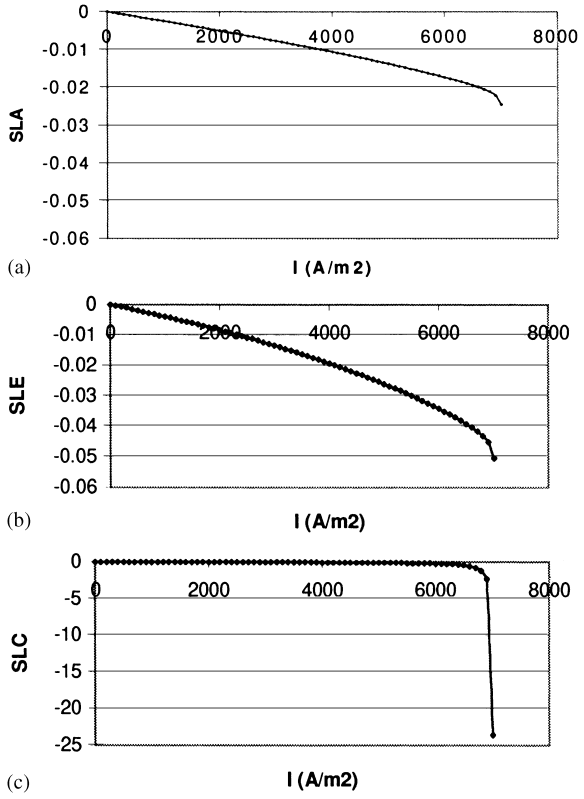

Fig. 10. (a) Sensitivity of cell voltage due to anode thickness (anode: 50 μm; cathode: 750 μm; electrolyte: 40 μm). (b) Sensitivity of cell voltage due to electrolyte thickness (anode: 50 μm; cathode: 750 μm; electrolyte: 40 μm). (c) Sensitivity of cell voltage due to cathode thickness (anode: 50 μm; cathode: 750 μm; electrolyte: 40 μm).

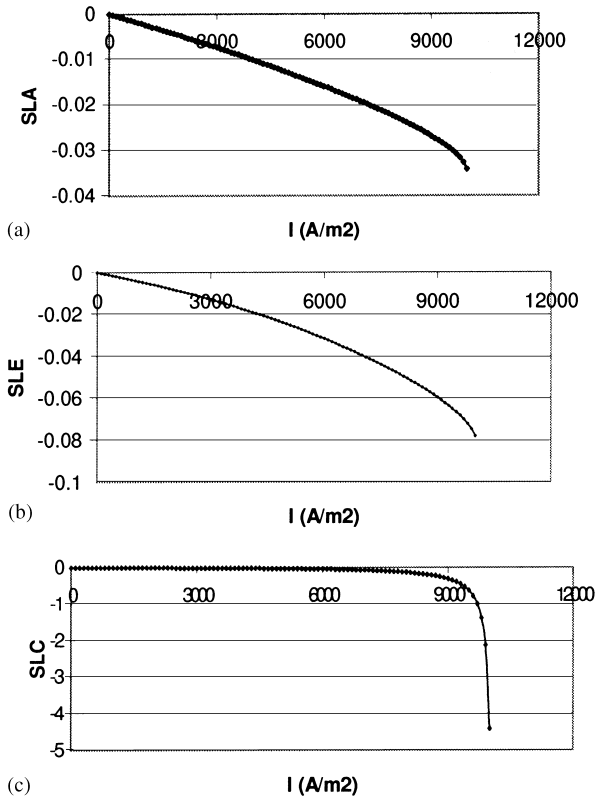

Fig. 11. (a) Sensitivity of cell voltage due to anode thickness (anode: 50 μm; cathode: 750 μm; electrolyte: 40 μm; p_c: 4 bar). (b) Sensitivity of cell voltage due to electrolyte thickness (anode: 50 μm; cathode: 750 μm; electrolyte: 40 μm; p_c: 4 bar). (c) Sensitivity of cell voltage due to cathode thickness (anode: 50 μm; cathode: 750 μm; electrolyte: 40 μm; p_c: 4 bar).

5. Summary and conclusions

It was felt that a generalized cell voltage–current density model could be important and useful for researchers who are working on SOFCs. Much effort in this study has been devoted to the development of this generalized model based upon thermodynamic principles whereby the irreversibility term in the steady flow thermodynamic system is manipulated electrochemically and replaced by the overall polarization.

This paper points out the applicable range of the Tafel equation and the simplified linear current–potential expression of the Butler–Volmer model which are easily mis-used. If 5% of error relative to the Butler–Volmer model is allowed for both cases, the activation overpotential for the Tafel equation should be more than 0.28 V and for the linear expression, <0.1 V. To generalize the cell voltage–current density model, the original Butler–Volmer expression is used in the calculation of activation polarization in conjunction with the consideration of both ordinary and Knudsen diffusion in the calculation of concentration polarization.

To develop a high-performance SOFC, the selection of a particular cell component as the support/substrate of the fuel cell can be the determining factor. Our study shows that the performance of an anode-supported cell is superior to that of an electrolyte-supported cell or a cathode-supported cell for the same materials used, same electrode kinetics and same operational constraints. Results show that when all three components are of the same thickness, the sensitivity of cell voltage due to the change of electrolyte thickness is the highest, then sensitivity of cell voltage due to the change of cathode thickness and finally the sensitivity of cell voltage due to the change of anode thickness. Reducing all three component thicknesses causes, in general, reduced sensitivity strength with an improved operating current density range. The study also reveals that a cathode-supported cell is no way better than an anode-supported cell for high performance fuel cell design even under elevated pressure conditions at the cathode compartment to compensate for the serious cathode concentration overpotential loss.

References

[1] S. Elangovan, J. Hartvigsen, A. Khandkar, R.M. Privette, K.E. Kneidel, J. Power Sources 71 (1998) 354–360.

[2] G.T. Lee, F.A. Sudhoff, Fuel cell/gas turbine system performance studies, in: Proceedings of Fuel Cells'96 Review Meeting, FETC Publications, Department of Energy, USA, 1996.

[3] Z. Takehara, K. Kanamura, S. Yoshioka, J. Electrochem. Soc. 136 (1989) 2506.
[4] K. Kanamura, S. Yoshioka, Z. Takehara, J. Electrochem. Soc. 138 (1991) 2165.
[5] C. Berger, Handbook of Fuel Cell Technology, Prentice-Hall, Englewood Cliffs, NJ, 1968.
[6] A.L. Hines, R.N. Maddox, Mass Transfer: Fundamentals and Applications, Prentice-Hall, Englewood Cliffs, NJ, 1985.
[7] C.J. Geankoplis, Mass Transport Phenomena, Holt, Rinehart & Winston, New York, 1972.
[8] K. Huang, M. Feng, J.B. Goodenough, J. Electrochem. Soc. 144 (1997) 3620.
[9] T. Ishihara, M. Honda, T. Shibayama, H. Minami, H. Nishiguchi, Y. Takita, J. Electrochem. Soc. 145 (1998) 3177.
[10] R. Maric, S. Ohara, T. Fukui, H. Yoshida, M. Nishimura, T. Inagaki, K. Miura, J. Electrochem. Soc. 146 (1999) 2006.
[11] P. Costamagna, P. Costa, V. Antonucci, Electrochim. Acta 43 (1998) 375–394.